

The unique dynamics of the Pacific Hemisphere mantle and its signature on seismic anisotropy

C. Gaboret^a, A.M. Forte^{b,*}, J.-P. Montagner^a

^a *Institut de Physique du Globe de Paris, Département de Sismologie, Paris, France*

^b *Department of Earth Sciences, University of Western Ontario, B&G Building, London, ON, Canada N6A 5B7*

Received 23 January 2002; received in revised form 26 April 2002; accepted 15 January 2003

Abstract

The portion of Earth's mantle lying below the hemispherical region occupied by the Pacific Ocean basin is characterized by a unique style of convection. The unique dynamics below the 'Pacific Hemisphere' are revealed by analyzing the mantle flow predicted on the basis of high-resolution seismic images of mantle structure. In the Pacific Hemisphere we find a dome-like upwelling, originating in the lower mantle, which actively transports material into the upper mantle. A unique aspect of this flow, found only in the Pacific Hemisphere, is a 'demi-tour' or U-turn of the circulation which occurs in the shallow mantle, west of the East Pacific Ridge. This 'demi-tour' connects the westward movement of the Pacific plate to the dome-like upwelling below the central Pacific Ocean and it also provides an explanation for the asymmetric distribution of seismic anisotropy on either side of the ridge axis. In a global analysis of the correlation between mantle flow and seismic anisotropy, we find the strongest agreement occurs in the Pacific Hemisphere mantle.

© 2003 Elsevier Science B.V. All rights reserved.

Keywords: Pacific hemisphere; East Pacific Rise; South Pacific Superswell; Mega-plume

1. Introduction

As was recognized in the earliest anisotropy studies in the Pacific Ocean basin [1], seismic anisotropy may provide essentially direct information about the convection-induced deformation of minerals comprising the upper mantle. The underlying basis for this relationship is the strong intrinsic anisotropy of the dominant constituent

minerals in the upper mantle, specifically olivine ($(\text{Mg,Fe})_2\text{SiO}_4$ and pyroxene $(\text{Fe,Mg,Ca})\text{Si}_2\text{O}_6$ [1,3–5]. In the presence of large-scale flow-induced deformation, these anisotropic minerals will be strained, resulting in a preferential orientation of their crystal axes [2–7]. If this lattice-preferred orientation (LPO) is organized over sufficiently long length scales it can be detected by seismic waves, and consequently seismic anisotropy may effectively provide maps of past or present-day mantle-flow velocities [1,8–11].

In this study we focused on the convective circulation, and its relationship to seismic anisotropy, in the Pacific Hemisphere using tomography-

* Corresponding author. Tel.: +1-519-661-3188;

Fax: +1-519-661-3198.

E-mail address: aforte@uwo.ca (A.M. Forte).

based mantle-flow models [12]. The Pacific plate constitutes an essentially uniform surface boundary and consequently theoretical modeling of flow in the Pacific Hemisphere should be less complex than in sub-continental mantle where there may be interactions with continental roots leading to the development of complex patterns of anisotropy [13–15] whose interpretation may be further complicated by the presence of ‘frozen-in’ or fossil anisotropy in the continental lithosphere [10,13,16]. The prevalence of fossil anisotropy is unclear, as there is some evidence suggesting a link between seismic anisotropy and contemporaneous deformation in the sub-continental mantle, for example below southern Africa [17] or below the western United States [18].

The special character of mantle flow and the associated seismic anisotropy in the Pacific Hemisphere is highlighted by recent discoveries of unique manifestations of mantle anisotropy in this region. Of particular interest is the strong asymmetry across the East Pacific Rise (EPR) [19,20] and the strong anisotropic signal in the central Pacific [21] (also seen in an earlier study [11], plate 2), with a westward offset that increases with depth [22].

Theoretical modeling of strain-induced seismic anisotropy generated by mantle flow has to date been carried out in two-dimensional Cartesian [23–26] or cylindrical [27] geometries. A more complete understanding of the information provided by seismic anisotropy requires an extension of mantle-flow modeling to three-dimensional (3-D) spherical geometry, with an appropriate model of mantle rheology and with a realistic distribution of buoyancy forces to drive the mantle circulation. In this study we employed a recent global model of seismically inferred anisotropy [28] to examine the extent to which anisotropy may be simply interpreted in terms of mantle-flow velocities or strain rates predicted by recently developed tomography-based 3-D flow models [12]. The initial goal of this testing is to determine to what extent observations of seismic anisotropy can be used to constrain mantle-flow models, with the ultimate goal to understand how mantle convection generates this anisotropy. Progress in this direction has been made in the most recent con-

vection modeling of radial anisotropy in the lower mantle [27]. In the following we will instead focus on flow-induced anisotropy in the upper mantle.

2. Mantle dynamics in the Pacific Hemisphere

2.1. Construction of the buoyancy-driven flow model

The development of a dynamical flow model requires knowledge of two main ingredients: the density distribution and the viscosity. The density anomalies we employed in our mantle-flow model are derived from seismic shear wave velocity heterogeneities in two recent global tomography models [21,29]. The conversion of relative perturbations of seismic shear velocity ($\delta V_s/V_s$) into equivalent relative density perturbations ($\delta\rho/\rho$) is accomplished using depth-dependent $\text{dln}\rho/\text{dln}V_s(r)$ conversion factors (Fig. 1a) obtained from inversions of convection-related geophysical data [12]. We note (Fig. 1b), with the exception of the transition zone region (400–1000 km depth), there is a relatively good agreement in the average amplitude of density anomalies derived from the two tomographic models using their respective conversion factors. Had we employed a single conversion profile, based for example on a simple thermal interpretation of mantle heterogeneity (dotted curve, Fig. 1a), the amplitude of the density anomalies inferred on the basis of the two tomography models would strongly differ throughout the mantle [12].

The two flow models we employ assume a mantle rheology represented by radial profiles of effective viscosity (Fig. 1c) which have also been derived by carrying out inversions of convection-related surface data [12,30]. The fits to the global convection data which have been employed to constrain the two flow models are summarized in Table 1. The inferred radial viscosity profiles (Fig. 1c) are characterized by strong variations with depth, which are well constrained by the convection data [12]. In particular, we note that these data require the presence of an asthenospheric low-viscosity channel in the depth range 100–300 km. A sub-lithospheric low-viscosity

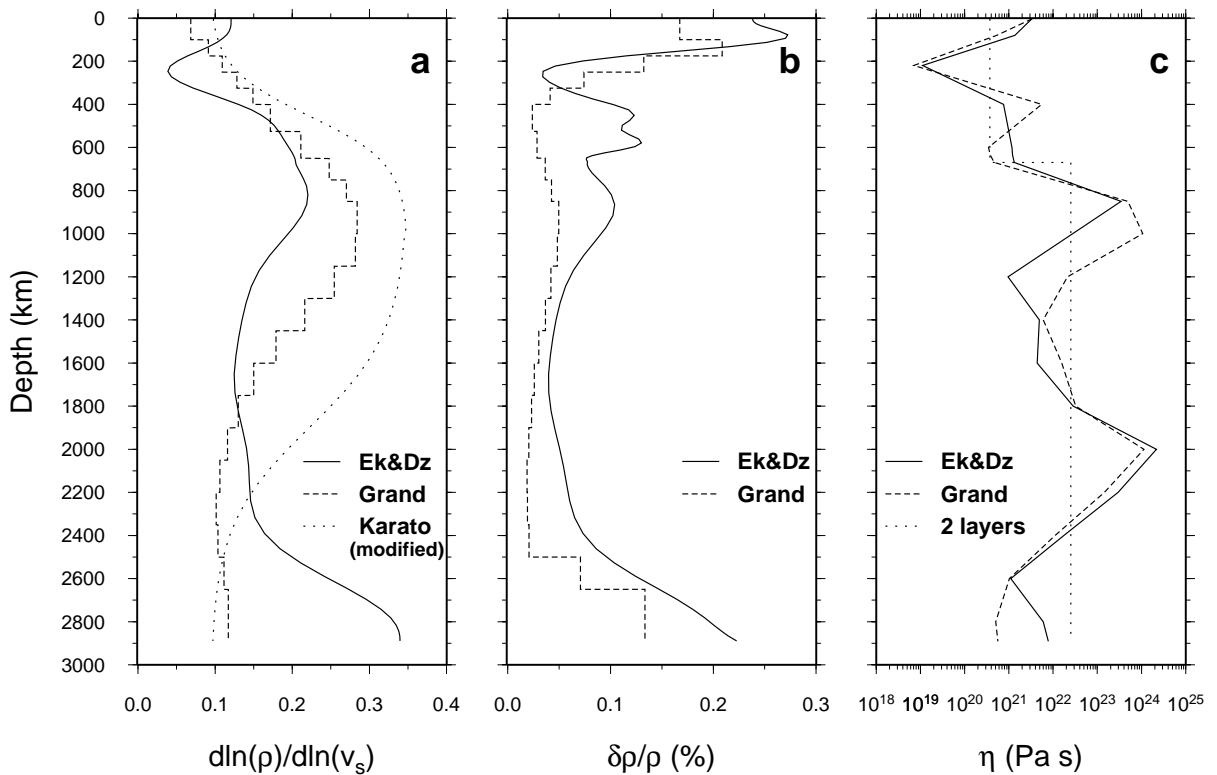


Fig. 1. Seismically inferred density anomalies and depth-dependent viscosity in the mantle. (a) The dotted line represents the velocity-to-density conversion profile $d\ln\rho/d\ln V_s$ estimated by Karato [51], using mineral physics theory and data, and later modified [56] to provide an improved match to heat flow and topography data. The dashed and solid lines represent the conversion profiles for the 3-D seismic tomography models of Grand [29] and Ekström and Dziewonski [21], respectively, which have been derived from inversions of convection-related data [12]. (b) The root-mean-square amplitude of the density perturbations $\delta\rho/\rho$ derived from the two tomography models using their respective conversion factors shown in panel a. (c) The dashed and solid lines represent the radial profile of effective viscosity inferred in inversions of global convection data [12] based on the tomography models of Grand and Ekström and Dziewonski, respectively. The dotted line represents a two-layer viscosity profile obtained by separately averaging the upper-mantle and lower-mantle viscosity variations in the profile (dashed line) inferred on the basis of Grand's tomography model.

layer has previously been inferred under the South Pacific Superswell (SPS) on the basis of the observed ratio between geoid and bathymetry anomalies in this region [31–33]. As described below, the strongly reduced mantle viscosity we infer in the asthenosphere has a strong impact on flow dynamics in the Pacific Hemisphere.

A distinct feature of the mantle-flow model we employ is that the plate motions are predicted rather than imposed. There are two distinct approaches for including plates in a dynamically consistent manner: (i) the torque-matching approach [34], which is based on earlier force-balance models of plate motions [35], and (ii) the

buoyancy projection method [36,37]. Both approaches treat the plates as rigid bodies and the geometry of the plates is prescribed at the outset. In both cases, however, the movements of the plates are not prescribed: they are predicted on the basis of the 3-D distribution of density anomalies throughout the mantle. In this study we employ the second approach and the plate geometries and corresponding projection operators [37] are represented in terms of spherical harmonic basis functions up to degree and order 64. The buoyancy-driven mantle flow, constrained only by the present-day plate geometry [38], produces plate movements which include both poloidal

Table 1
Fits to global convection data^a provided by mantle-flow models

3-D mantle Model	Gravity ^b [$l=2-20$]	Topography ^c [$l=1-20$]	Divergence ^d [$l=1-32$]	Vorticity ^d [$l=2-32$]
Grand ^e	33% (64%) ^f	48%	59%	21%
Ek & Dz ^e	43% (71%) ^f	22%	69%	40%
Grand ^g	21% (38%) ^f	27%	41%	16%

^a All fits are expressed in terms of variance reduction.

^b The observed free-air gravity anomalies are calculated using the (non-hydrostatic) geopotential derived from satellite data [54].

^c The dynamic surface topography is obtained by removing the contribution of isostatically compensated crust from observed surface topography [55].

^d The NUVEL-1 plate motion data [38] are represented here in terms of the horizontal divergence and radial vorticity of the plate velocity field. (We exclude the $l=1$ components of vorticity, which correspond to the net lithosphere rotation.)

^e The density perturbations are derived on the basis of the associated $d\ln\rho/d\ln V_S$ profiles (Fig. 1a) inferred in inversions of the convection data [12].

^f The numbers in parentheses are the variance reductions to the equivalent non-hydrostatic geoid anomalies derived from satellite data [54].

^g The two-layer viscosity model (dotted curve, Fig. 1c), along with the $d\ln\rho/d\ln V_S$ profile in Fig. 1a labeled ‘Karato’, are used in this viscous-flow calculation.

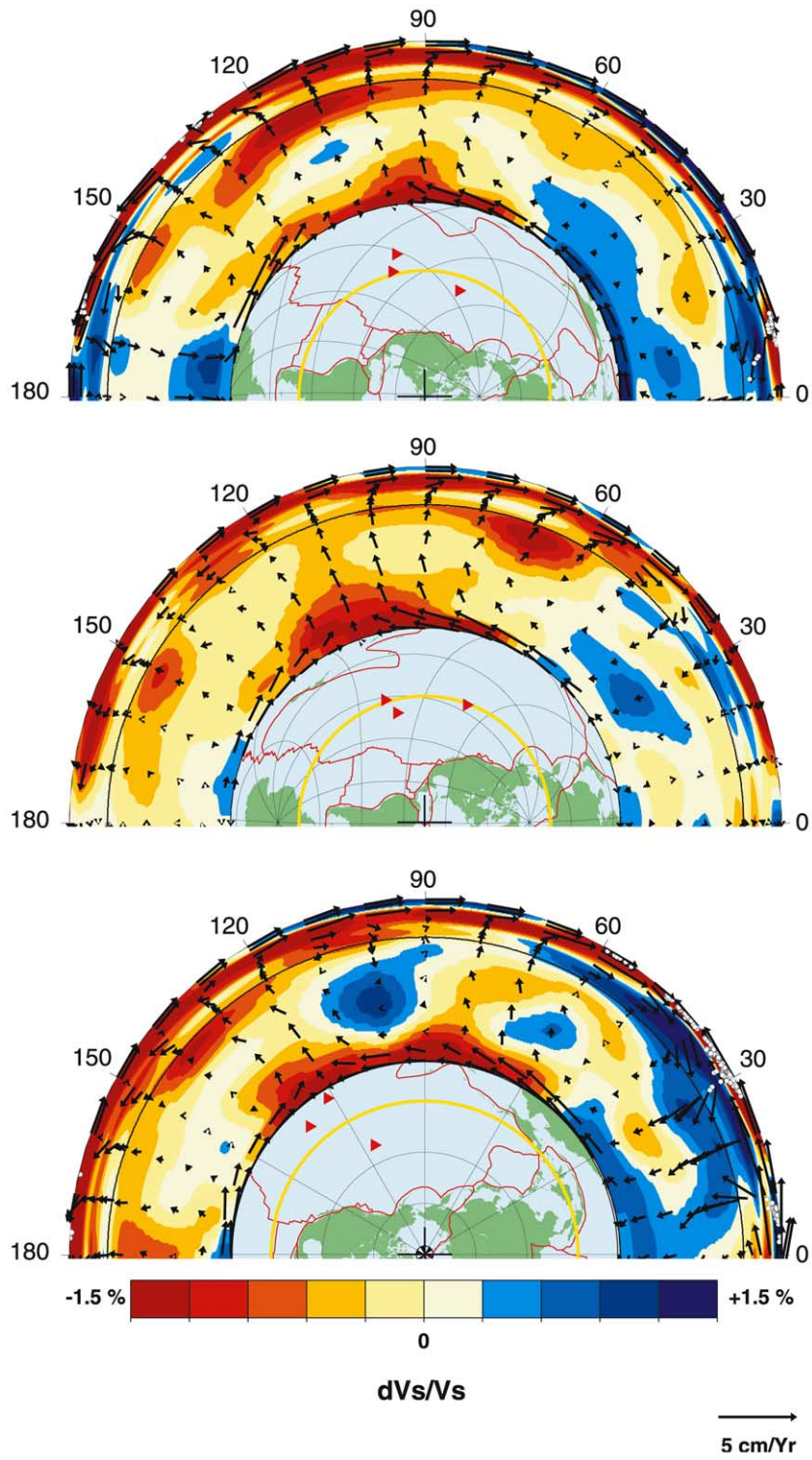
and toroidal components. This method for predicting plate motions avoids the creation of physically unrealistic stress fields in the mantle which will arise when mantle flow driven by a priori plate velocities is superimposed on buoyancy-driven internal flow whose geometry is not necessarily consistent with that of the plates. This technique, incorporated in a reformulated mantle-flow theory [30], allows us to model flow, stress and deformation in the mantle. A more detailed description of the basic theory and numerical methods we employed here to model buoyancy-induced mantle flow may be found in previous studies [30,35,36].

2.2. Unique flow dynamics below the Pacific plate

The mantle-wide circulation we predict on the

basis of the buoyancy forces derived from the Ekström and Dziewonski [21] tomography model is illustrated in several cross-sections in Fig. 2. The black arrows represent the projections of the (3-D) flow field onto the plane of the cross-sections (flow components perpendicular to these planes are not shown). The rotation of the flow vectors out of the plane of the cross-sections, especially in the near-surface region where there is significant toroidal flow associated with the plate motions, may appear as a partial ‘decoupling’ of the surface flow relative to deeper mantle flow. From a dynamical perspective, the impact of the very-low-viscosity channel in the asthenosphere (Fig. 1c) permits a strong vertical gradient of the horizontal component of the buoyancy-driven flow field in this channel. This viscosity-modulated gradient is evident in all the cross-sections (Fig. 2) and it also

Fig. 2. Mantle heterogeneity and convective flow in the Pacific Hemisphere. Three whole-mantle cross-sections through the Ekström and Dziewonski tomography model [24] along great circles. The color contours represent the relative perturbations in seismic shear velocity $\delta V_S/V_S$ identified by the bottom scale bar. The great-circle slices are indicated by yellow lines in each of the inset maps. Also shown in the inset maps are red triangles which represent the locations of three Pacific hotspots: Hawaii (Kilauea), Tahiti (Mehetia) and Marquesas. The superimposed black arrows in the cross-sections represent the mantle-flow velocities (scale shown at bottom right) predicted [21] on the basis of the buoyancy forces derived from the Ekström and Dziewonski tomography model. The small white circles represent the location of earthquake hypocenters obtained from a compilation of global seismicity [39], in which we selected all natural events over the past 30 years with $M_s \geq 5.5$. All events in a swath extending $\pm 1^\circ$ out of the plane of the cross-sections are plotted.



gives rise to the appearance of a decoupling of the near-surface and deeper flow fields.

The background color contours in Fig. 2 represent the seismic shear-velocity heterogeneity [21] in the plane of the cross-sections. The driving buoyancy forces in the mantle are related to this seismic heterogeneity via the $d\ln\rho/d\ln V_S$ conversion profiles (Fig. 1a). The mantle circulation pattern in Fig. 2 is clearly dominated by a very long horizontal length scale, which reflects the dominant influence of the very long wavelength heterogeneity in the seismic tomography models. In some locations (e.g. in the lower cross-section at 60°), this large-scale flow dominates or ‘overrides’ the flow that might otherwise be created by the smaller-scale mantle heterogeneity. It is clear, however, that the flow velocities do agree with the trajectories of subducting plates along Wadati–Benioff zones (white circles, Fig. 2), which were delineated using catalogs of seismic hypocenter locations [39]. These flow trajectories below subduction zones were not imposed a priori constraints in our mantle circulation models and they therefore provide a useful independent test of the plausibility of these models.

The predicted mantle-flow field (Fig. 2) reveals a large-scale upwelling, or ‘mega-plume’, in the deep mantle below the SPS. The shape and large horizontal extent of this mega-plume resembles the doming regime observed in recent fluid mechanical experiments of thermochemical convection [40]. As shown previously in a deep mantle study [12], the main control on the length scale and shape we predict for this domed upwelling is the region of very high viscosity near 2000 km depth (Fig. 1c). In the upper-mantle low-viscosity channel we also observe a remarkable ‘demi-tour’ (U-turn) [43] of the flow field (top and bottom cross-section, Fig. 2) in which the mantle upwelling focused below the SPS is sharply deflected laterally and rises below the EPR, where the flow then couples to the SE–NW motion of the Pacific plate. This ‘demi-tour’ is made possible by the greatly reduced viscosity in the asthenospheric channel. The ‘demi-tour’ arises so that the predicted large-scale flow ascending below the SPS can be accommodated by similarly large-scale sur-

face flow which is coupled to the Pacific plate motion.

To further clarify the material transport associated with this flow ‘demi-tour’ below the Pacific plate, we considered two initially adjacent particles at the base of the upper mantle which were placed below the eastern edge of the surface expression of the SPS (Fig. 3). The trajectories of these particles are calculated with a second-order accurate predictor–corrector algorithm [41] in which we employ time (and hence space) steps which ensure that local errors are kept small (less than 1 part in 10^{12}) in each iteration. We find that this provides a high spatial resolution for the particle trajectories (with space steps less than 1 km). We then verified the predicted particle trajectories by carrying out a second calculation based on a high-accuracy advection algorithm [42].

The predicted trajectories (Fig. 3) show that as both particles ascend across the upper-mantle transition zone they are progressively deflected eastward. When the particles reach the low-viscosity asthenosphere their trajectories are nearly sub-horizontal and their horizontal transport speeds are maximum. As they approach the surface, west of the EPR, one of the particles accomplishes a ‘demi-tour’ and follows the westward movement of the Pacific plate while the other particle continues eastward and follows the Nazca plate motion. As a consequence of this ‘demi-tour’, there is a clear shift of the mantle upwelling center to a location west of the EPR.

The predicted particle trajectories in Fig. 3 show that the mass flux required to sustain the rapid divergence of the EPR begins at the base of the upper mantle directly below the SPS, and the flow must therefore travel horizontally at high rates in the asthenosphere channel. This rapid horizontal asthenospheric flow is also very evident in Fig. 2. This result supports a recent study of lateral variations of seismic attenuation in the upper mantle, in which it is proposed that the lower-mantle superplume below the Pacific (and the other below Africa) extends upward across the upper-mantle transition zone and is then deflected horizontally below the lithosphere [44].

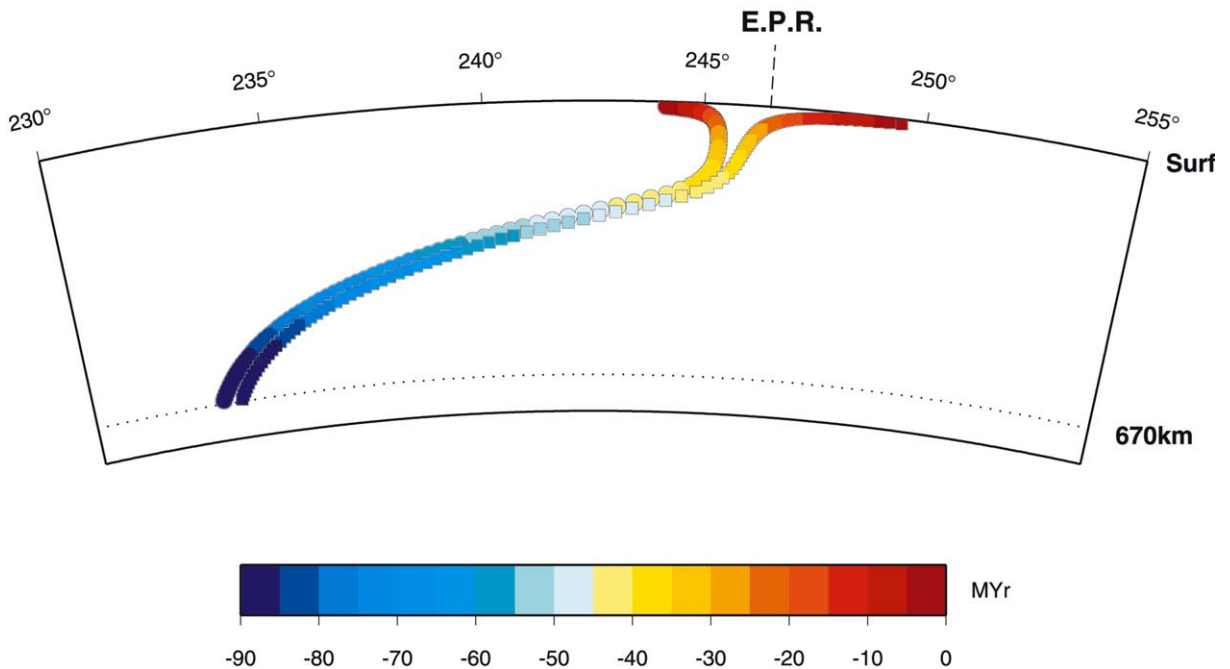


Fig. 3. The ‘demi-tour’ of mantle flow below the Pacific plate. Here we observe the trajectories of two nearby particles released in the mantle-flow field and initially located below the eastern edge of the South Pacific Superswell (starting position is: depth = 670 km, latitude = -20° , longitude = 234°). In the advection calculation we assumed a time-invariant flow field, equal to the predicted present-day mantle flow, and the elapsed time (shown by scale bar at bottom) is represented relative to present-day (time 0). The mantle-flow model used in this advection calculation is the same as that in Fig. 2. The ‘demi-tour’ or U-turn of one of the particle paths, occurring in the shallow mantle west of the East Pacific Ridge (EPR), is clearly visible.

3. Mantle deformation and seismic anisotropy in the Pacific Hemisphere

3.1. A flow-related proxy for LPO

It is generally accepted that the development of coherent mineral alignment in a polycrystalline aggregate will depend on its deformation history. This understanding forms the basis of early investigations of the relationship between flow-induced deformation and seismic anisotropy [23]. Subsequent calculations [25] suggested that an analysis of the present-day finite strain tensor should be sufficient for modeling LPO and seismic anisotropy in the mantle. The predicted anisotropy was found to be only weakly dependent on the actual deformation path of the polycrystal. These models suggested that the relative lengths of the principal axes of the finite strain ellipsoid may be used to estimate seismic anisotropy [25]. If we assume that

the present-day deformation of mantle material produced by the large-scale flow we are modeling is slowly varying over time, then we may employ the principal axes of the rate-of-strain tensor to approximate the corresponding geometry of the finite-strain tensor. This approximation will not be applicable in regions with a complicated, rapidly changing deformation history. In this study we will therefore adopt the principal axis (i.e. the eigenvector corresponding to the largest eigenvalue) of the rate-of-strain tensor as a proxy for the LPO produced by the mantle convective flow. Geometrically speaking, this axis corresponds to the direction of maximum flow-induced extension or stretching of mantle rocks.

There are a number of mineral physics considerations which may complicate the relationship between seismic anisotropy and our adopted proxy for LPO. Phase changes, either solid–solid (e.g. the exothermic transition at 400 km depth)

or solid–liquid (e.g. partial melting), may have a major impact on LPO. Dynamic recrystallization may also have a large effect on the evolution of LPO in the mantle [2]. A recent theoretical study [45] shows that the impact of dynamic recrystallization on LPO depends on several factors, such as the hardness of the individual slip systems in mineral crystals. This hardness may determine whether mineral fabric is ultimately aligned with the plane of externally imposed shear, as revealed in one experimental study [6], or aligned with the finite strain axis, as shown in later experiments [7]. The strength of the slip systems is uncertain and may be affected by the water content of mantle rocks, the importance of which has been highlighted by a new study [46]. Additional uncertainty arises when extrapolating the results of these experimental studies to the mantle. Most experimental and theoretical analyses of LPO have been carried out under simplified deformation geometries, involving simple or pure shear. The deformation predicted on the basis of our mantle-flow models is fully 3-D and is considerably more complex. In view of these multiple uncertainties, one must be cautious in evaluating the applicability of our chosen proxy for LPO and in interpreting its relationship to seismically inferred mantle anisotropy, which is presented next.

3.2. Predicted deformation and seismically inferred anisotropy

To determine the impact of the predicted flow on mantle deformation below the Pacific plate, we first investigated the relationship between seismically inferred radial anisotropy and the vertical component of the maximum flow-induced stretching (extension) rates. A previous global tomography model [21] suggests that radial anisotropy below the Pacific plate is largest in the 100–200 km depth interval (Fig. 4). We compared this radial anisotropy with the predicted vertical deformation at 160 km depth and found a good anticorrelation (Fig. 4) between the two fields, particularly in the sub-oceanic mantle below the Pacific plate. In the central Pacific the radial anisotropy has a particularly large amplitude [11,21], corresponding to $\delta V_{SV} < \delta V_{SH}$, and this would appear

to be in accord with the model prediction that vertical deformation is minimal, which implies a dominant horizontal, rather than vertical alignment of LPO in this region. In contrast, on the periphery of the Pacific plate (Fig. 4) the flow model predicts peak amplitudes in buoyancy-driven vertical deformation rates. The sub-oceanic mantle below the Antarctic and Nazca plates is also characterized by small rates of vertical stretching, as below the central Pacific, and yet the radial anisotropy is very weak, with $\delta V_{SV} \approx \delta V_{SH}$. This discrepancy further reinforces the previous inference [21] that radial anisotropy in the Pacific upper mantle is anomalous.

In the eastern Pacific (Fig. 4), in particular along the EPR, there is a strongly pronounced asymmetry with maximum deformation concentrated west of the ridge axis and very little vertical deformation east of the ridge. This asymmetry in the predicted vertical deformation rates, associated with the ‘demi-tour’ of shallow mantle flow (Fig. 3), provides a natural explanation for the corresponding asymmetry of seismic anisotropy inferred from shear wave splitting studies [19] in the MELT study region [20] of the EPR. The origin of this asymmetry in terms of upper-mantle flow connecting the SPS to the EPR has also been hypothesized in previous studies [19,22,47,48].

It is generally supposed that upper-mantle azimuthal anisotropy, which may be inferred in seismic surface wave studies [8,11,49], provides a signature of the horizontal component of flow-induced deformation. We examined this relationship in the Pacific Hemisphere mantle by comparing a recent model of azimuthal seismic anisotropy [28] with the horizontal component of the maximum extension axis predicted by the two tomography-based flow models [12] used in this study. The correspondence between anisotropy and mantle deformation at 200 km depth (Fig. 5) is quantified locally in terms of (the cosine of) the angular offset between between the fast axis of seismic V_{SV} velocity (blue lines, Fig. 5) and the axis of the (horizontal component of) maximum extensional rate (red lines, Fig. 5).

The overall agreement between the model of seismic azimuthal anisotropy and our proxy for

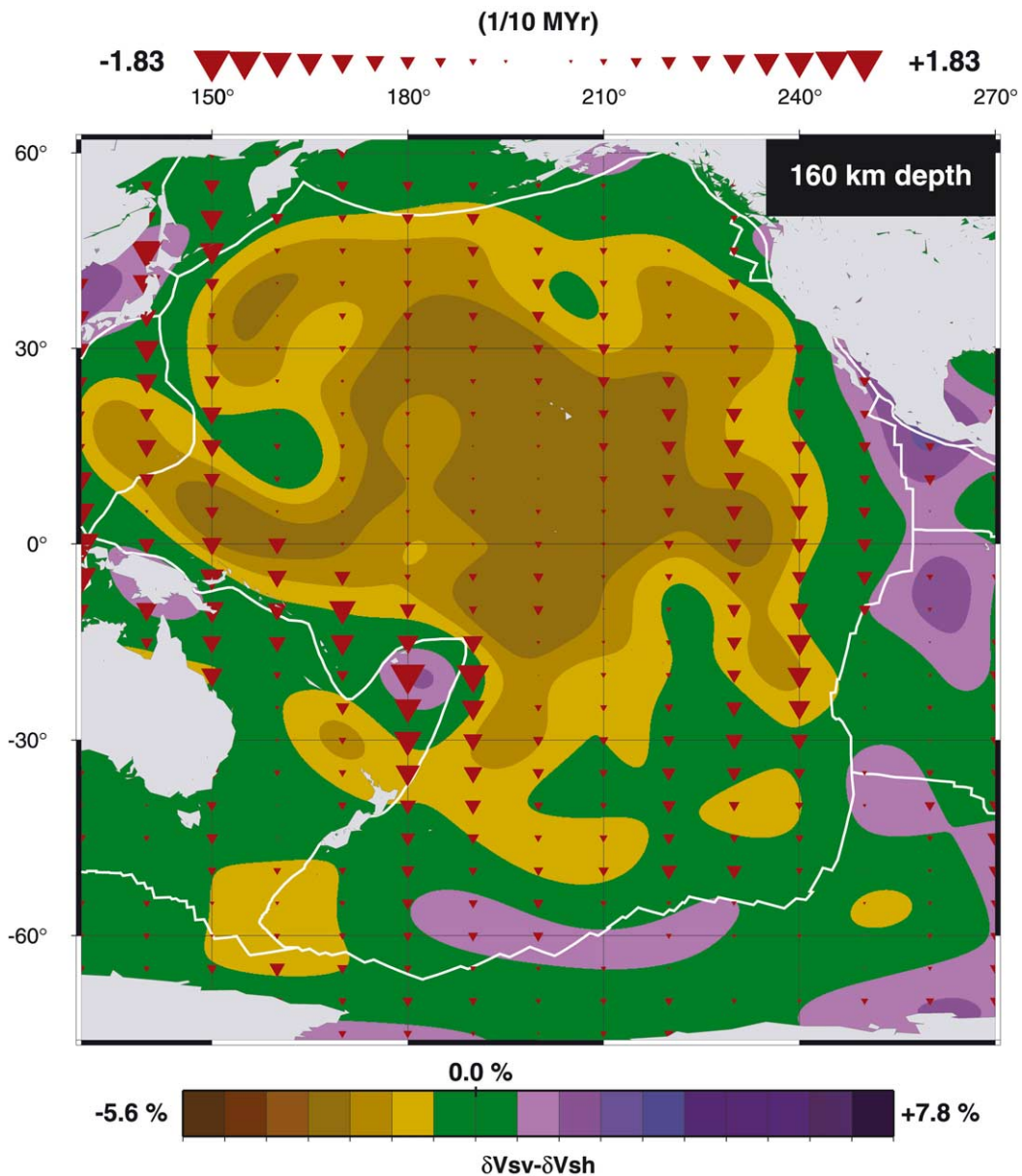


Fig. 4. Radial seismic anisotropy and vertical rates of deformation at 160 km depth in the Pacific Hemisphere mantle. The color contours (scale bar at bottom) represent the radial anisotropy, $\delta V_{SV}/V_{SV} - \delta V_{SH}/V_{SH}$, determined by Ekström and Dziewonski [21]. The red triangles represent, at the same depth, the vertical component of the maximum rate of stretching (scale bar at top) predicted on the basis of mantle flow driven by the buoyancy forces derived from the isotropic heterogeneity in the Ekström and Dziewonski tomography model.

LPO (Fig. 5) is fairly good, especially in the mantle to the north/west of the ridge axis, which separates the Antarctic/Nazca plates from the Pacific plate. (A quantitative measure for the overall

agreement will be introduced below.) We note that in the higher latitudes, below the northern and western portions of the Pacific plate, there are regions in which the correlation between ani-

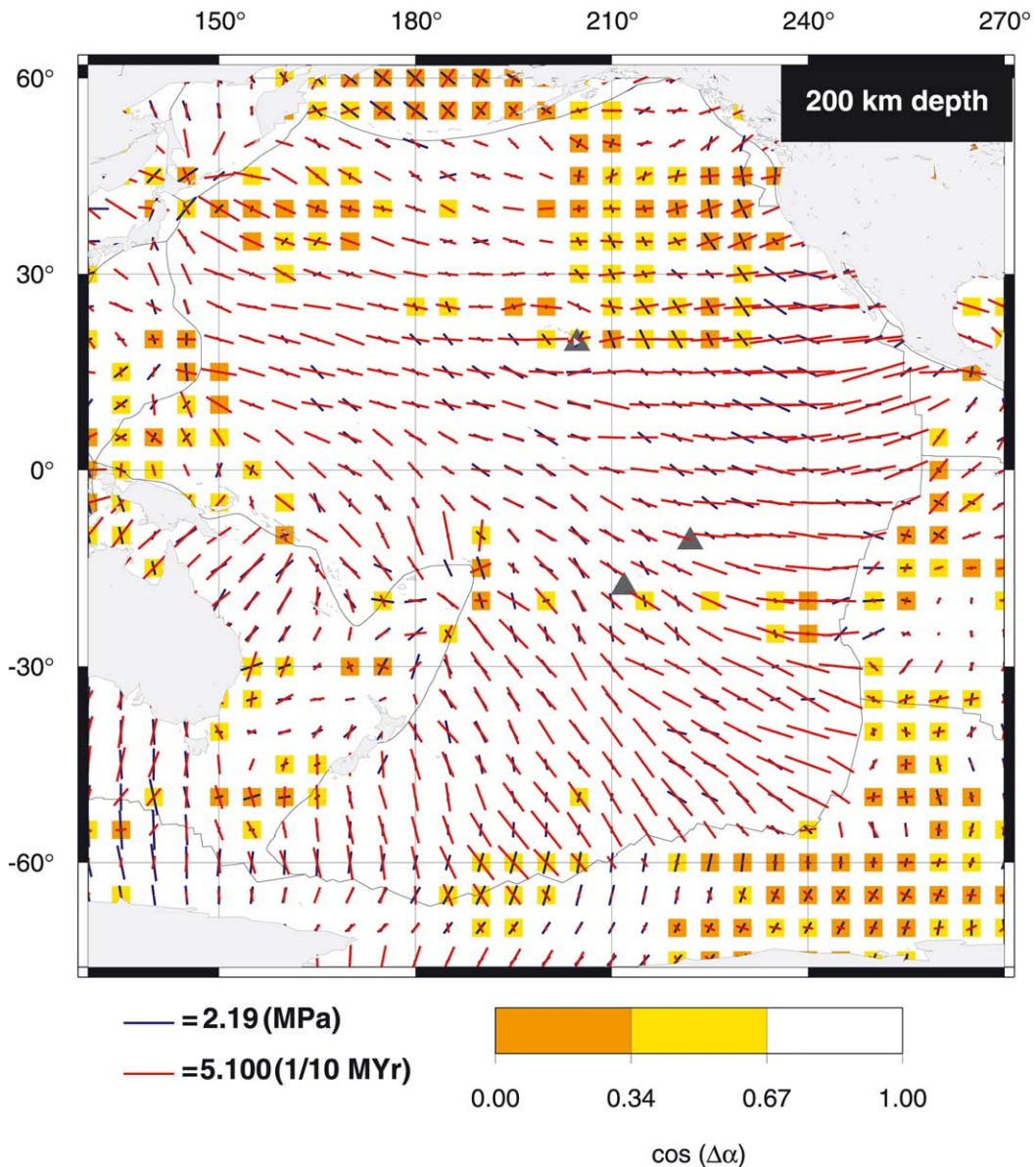


Fig. 5. Azimuthal anisotropy and horizontal deformation rates at 200 km depth in the Pacific Hemisphere mantle. The horizontal components of the maximum stretching rates (red lines, scale shown at bottom of map) are predicted with a flow model [12] based on Grand's tomography model [29]. The azimuthal seismic anisotropy inferred in a recent global tomography model [28] is represented by the blue lines, which identify the axis of fast V_{SV} velocity. The amplitude of the anisotropy is quantified in terms of the seismic G parameter (scale shown at bottom of map), which is the elastic modulus that determines the amplitude and orientation of the fast propagation direction for surface Rayleigh waves [11]. The agreement between the direction of azimuthal anisotropy and the direction of horizontal stretching rate is quantified in terms of the cosine of their angular offset. The white cells represent good agreement and the orange cells represent poor agreement.

sotropy and deformation is poor. As noted above (Section 3.1), there are a variety of physical effects which may intervene to obscure the relationship between anisotropy and deformation. One additional factor which may play a role here, especially in the northwestern Pacific, is the presence of fossil anisotropy in the older portions of the oceanic lithosphere [50]. In such regions, the alignment of mineral fabric and azimuthal anisotropy may not be that expected from an analysis of present-day mantle flow. The fields shown in Fig. 5 correspond to a depth of 200 km, therefore it is unclear to what extent fossil anisotropy in the lithosphere may be a factor. The answer will depend on the actual magnitude of this fossil anisotropy and on the depth-dependent resolving power of the seismic data.

For many locations (Fig. 5) displaying large angular offsets between azimuthal anisotropy and predicted deformation, the amplitude of the predicted deformation and/or of the seismically inferred anisotropy is relatively small. This is the case below the Nazca and Antarctic plates. From a dynamical perspective, these areas should be less important than other regions where the amplitudes are high and therefore any misfit to the seismic anisotropy axes may be considered to be more significant. In developing a quantitative measure of the overall spatial correspondence between the two fields we should therefore include a weighting based on the local amplitudes of the fields. One such measure is the cross-correlation (cc), defined by the following formula:

$$cc = \frac{\sum_{i=1}^N \lambda_i \gamma_i |\cos(\Delta\alpha)|}{\sqrt{\sum_{i=1}^N \lambda_i^2} \sqrt{\sum_{i=1}^N \gamma_i^2}}$$

where N is the total number of geographic samples, λ_i is the magnitude of the horizontal maximum stretching, γ_i is the magnitude of the azimuthal anisotropy and $\Delta\alpha$ represents the angular difference between their associated directions.

A summary of the cc between azimuthal anisotropy and our LPO proxy (the horizontal component of maximum extension rate) is provided in Fig. 6, which focuses on the top 300 km of the mantle, where azimuthal anisotropy inferred on the basis of seismic surface waves [28] is best re-

solved. In this figure we also summarize the cc between azimuthal anisotropy and the predicted horizontal component of the mantle-flow field. A number of previous seismological studies have explored the extent to which azimuthal anisotropy may be used as a direct proxy for mantle flow [1,5,8,9,11]. The cc is calculated for the entire globe and for the Pacific Hemisphere mantle and we note, as expected (see introductory discussion), that there is better agreement in the Pacific Hemisphere (Fig. 6). At shallower depths (above 100 km) we also note that the cc between maximum extension rates and azimuthal anisotropy (Fig. 6b) is significantly less than it is for flow directions (Fig. 6a).

In view of the fair agreement (Figs. 5 and 6) between seismic anisotropy and our instantaneous, flow-related proxy for LPO, it appears that seismic anisotropy may be a potentially useful constraint on mantle-flow models. We have explored this possibility by attempting to construct other mantle-flow models, based on different radial viscosity profiles, which might yield even better fits to the seismically inferred anisotropy. We therefore considered a flow model based on a simple two-layer viscosity profile which was obtained by calculating viscosity averages in the upper and lower mantle, using the radial viscosity profile (dashed curve, Fig. 1c) inferred on the basis of Grand's tomography model [29]. The mantle density anomalies are derived from the shear velocity heterogeneity in Grand's model using a simple $d\ln\rho/d\ln V_S$ conversion profile (dotted curve, Fig. 1a) based on mineral-physics modeling [51]. Despite the relative simplicity of this new flow model, we note in Fig. 6 that it yields a significantly improved match between seismic anisotropy and our LPO proxy. This agreement is particularly good below the lithosphere, approaching correlation values of +0.75 in the Pacific Hemisphere mantle (Fig. 6b). The fits to the convection-related surface observables provided by this flow model are summarized in Table 1.

4. Conclusions

The flow predictions illustrated in Fig. 2 reveal

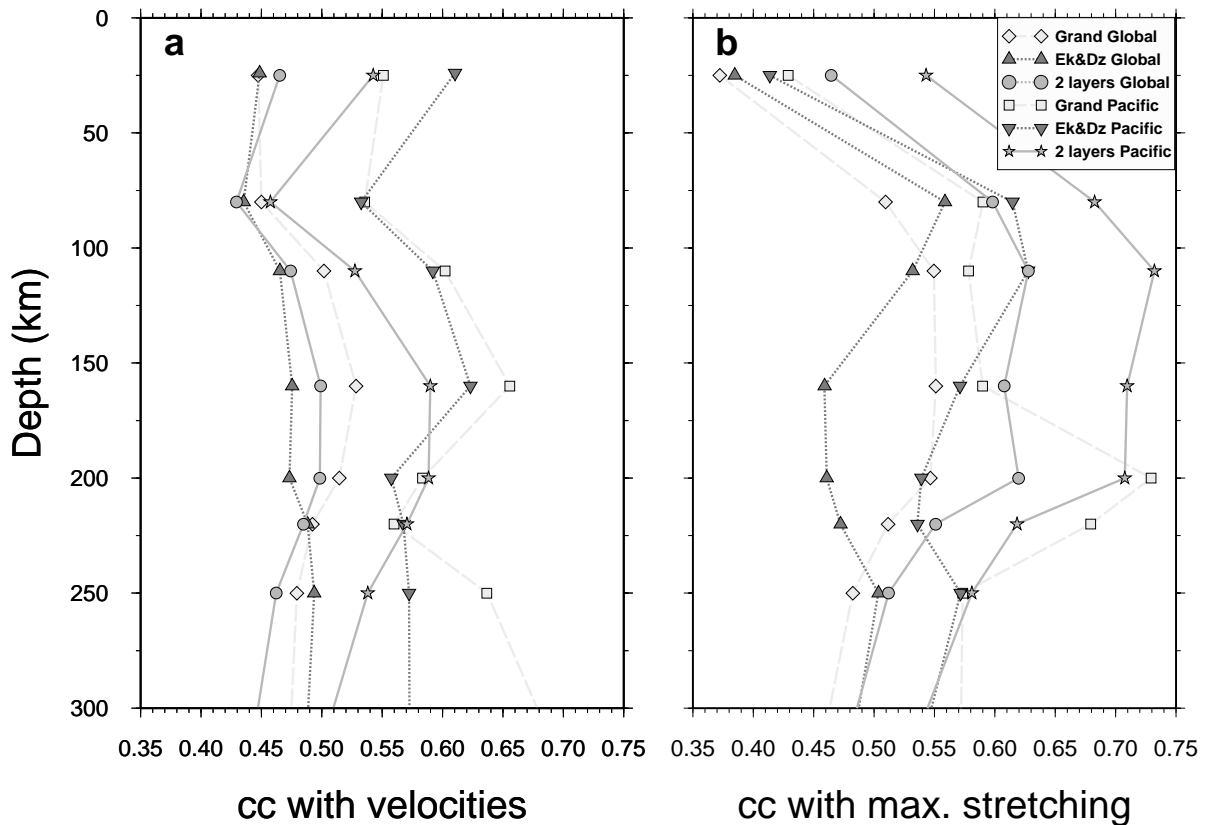


Fig. 6. Cross-correlation between azimuthal seismic anisotropy and horizontal deformation or flow as a function of depth. The global and Pacific Hemisphere cross-correlations cc are shown for predictions obtained on the basis of three mantle-flow models (see inset legend in frame b) which are constructed using the three viscosity profiles shown in Fig. 1c. The flow model employing the two-layer viscosity profile is based on the density anomalies derived from Grand's tomography model [29] and uses the $d\ln\rho/d\ln v_s$ profile estimated from mineral physics and geodynamic data (dotted line, Fig. 1a).

that the mantle circulation below the Pacific plate is driven by a large-scale buoyant upwelling which originates in the deep mantle below the SPS. The mass flux which sustains the rapid divergence of the EPR is mediated by the low-viscosity asthenosphere, which horizontally channels the upwelling flow below the SPS to the EPR. This connection between the ascending flow and the movement of the overlying Pacific plate produces a fundamental asymmetry in the pattern of mantle flow, giving rise to the pronounced 'demi-tour' (Fig. 3) of shallow particle trajectories just west of the EPR. This asymmetry in shallow flow beneath the EPR is also manifested as an asymmetry in our proxy for LPO, with predicted deformation rates which

are much stronger to the west of the EPR than they are to the east. As suggested earlier [43,47], this asymmetric deformation provides an explanation for the corresponding asymmetry in seismic anisotropy which was mapped in the MELT experiment [20].

The mantle-flow and deformation predictions obtained in this study are based on viscous flow calculations which assume a depth-dependent rheology. The temperature dependence of the effective viscosity of mantle minerals is well known (for example, [52]) and it implies that significant lateral variations in viscosity should be present throughout the mantle. The relative dynamical importance of lateral versus depth-dependent vis-

cosity variations in large-scale global flow models has been explored in previous studies [12,37]. These studies showed that in the presence of large-scale lateral viscosity variations, whose amplitude is comparable to that of the radial viscosity variations, the impact on predicted surface observables (e.g. topography and gravity anomalies) is relatively small. Nonetheless, it is possible that more focused, smaller scale-length lateral variability in viscosity may have a significant impact on local flow dynamics. We cannot discern this effect in the current tomography-based flow models, but this is a question that should be considered in future higher-resolution flow models. The tectonic plates themselves may constitute the most extreme manifestation of lateral viscosity variations [53] and, as discussed above (Section 2.1), the impact of these plates on mantle flow is at least accounted for in our global flow models.

Despite the significant uncertainties associated with the possible impact of lateral viscosity variations and mineral physics complexities (Section 3.1), we found a good correspondence (Figs. 5 and 6) between azimuthal seismic anisotropy and the principal (maximum) extension axis of the rate of strain ellipsoid. This suggests that this instantaneous signature of flow-induced mantle deformation is a reasonably good proxy for LPO in the upper mantle, at least in sub-oceanic regions. This further suggests that a detailed understanding of the past history of deformation may not be critical to our understanding of present-day LPO, except in regions with significant fossil anisotropy or complicated deformation histories. This observation, in combination with the recent results obtained in theoretical models of dynamic recrystallization [45], suggests to us that the continual re-setting of mineral fabric by the process of recrystallization plays an essential role in controlling the evolution of LPO. Finally, we also note that mantle-flow models based on different viscosity profiles provide distinctly different fits to azimuthal anisotropy (Fig. 6). We therefore expect that, in future studies, it should be possible to jointly invert convection-related surface observables (Table 1) along with seismically inferred anisotropy to obtain improved constraints on geodynamic models.

Acknowledgements

We acknowledge E. Kaminski and N. Ribe for many helpful discussions during our research. Discussions with A. Bonneville helped to clarify ideas. We thank two anonymous referees and M. Savage for their thorough and constructive reviews. A.M.F. is grateful for the hospitality and support provided by the Institut de Physique du Globe de Paris (IPGP) during the revision process. Support provided by the Canadian Natural Sciences and Engineering Research Council (NSERC) and the Canada Foundation for Innovation – Ontario Innovation Trust (CFI–OIT) is also acknowledged. A.M.F. also thanks the additional support provided by the Canadian Institute of Advanced Research – Earth System Evolution Program. This is IPGP Contribution No. 1892. [BW]

References

- [1] H. Hess, Seismic anisotropy of the uppermost mantle under the oceans, *Nature* 203 (1964) 629–631.
- [2] N.L. Carter, D.W. Baker, R.P. George Jr., Seismic anisotropy, flow, and constitution of the upper mantle, in: H.C. Heard, I.Y. Borg, N.L. Carter, C.B. Raleigh (Eds.), *Flow and Fracture of Rocks*, Geophys. Monogr. Ser. 16, American Geophysical Union, Washington, DC, 1972, pp. 167–19.
- [3] A. Nicolas, N.I. Christensen, Formation of anisotropy in upper mantle peridotites - a review, in: K. Fuchs, C. Froidevaux (Eds.), *Composition, Structure and Dynamics of the Lithosphere-Asthenosphere System*, Geodyn. Ser. 16, American Geophysical Union, Washington, DC, 1987, pp. 111–123.
- [4] S.I. Karato, Seismic anisotropy; mechanisms and tectonic implications, in: S.-I. Karato, M. Toriumi, (Eds.), *Rheology of Solids and of the Earth*, Oxford University Press, Oxford, 1989, pp. 393–342.
- [5] D.L. Anderson, *Theory of the Earth*, Blackwell, Boston, 1989.
- [6] S.Q. Zhang, S.I. Karato, Lattice preferred orientation in olivine due to shear deformation, *Nature* 375 (1995) 774–777.
- [7] M. Bystricky, K. Kunze, L. Burlini, J.P. Burg, High shear strain of olivine aggregates: Rheological and seismic consequences, *Science* 290 (2000) 1564–1567.
- [8] D.W. Forsyth, The early structural evolution and anisotropy of the oceanic upper mantle, *Geophys. J. R. Astron. Soc.* 43 (1975) 103–162.

- [9] T. Tanimoto, D.L. Anderson, Mapping convection in the mantle, *Geophys. Res. Lett.* 11 (1984) 287–290.
- [10] P.G. Silver, W.W. Chan, Shear-wave splitting and sub-continental mantle deformation, *J. Geophys. Res.* 96 (1991) 16429–16454.
- [11] J.-P. Montagner, Can seismology tell us anything about convection in the mantle?, *Rev. Geophys.* 32 (1994) 115–137.
- [12] A.M. Forte, J.X. Mitrovica, Deep mantle high viscosity flow and thermochemical structure inferred from seismic and geodynamic data, *Nature* 410 (2001) 1049–1056.
- [13] P.G. Silver, Seismic anisotropy beneath the continents: Probing the depths of geology, *Annu. Rev. Earth Planet. Sci.* 24 (1996) 385–432.
- [14] V. Babuška, J.-P. Montagner, J. Plomerová, N. Girardin, Age-dependent large-scale fabric of the mantle lithosphere as derived from surface-wave velocity anisotropy, *Pure Appl. Geophys.* 151 (1998) 257–280.
- [15] M.K. Savage, Seismic anisotropy and mantle deformation: What we learned from shear wave splitting?, *Rev. Geophys.* 37 (1999) 65–106.
- [16] R. Kind, G.L. Kosarev, L.I. Makeyeva, L.P. Vinnik, Observations of laterally inhomogeneous anisotropy in the continental lithosphere, *Nature* 318 (1985) 358–361.
- [17] L.P. Vinnik, R.W.E. Green, L.O. Nicolaysen, Recent deformations of the deep continental roots in southern Africa, *Nature* 375 (1995) 50–52.
- [18] M.K. Savage, P.G. Silver, Mantle deformation and tectonics: Constraints from seismic anisotropy in western United States, *Phys. Earth Planet. Inter.* 78 (1993) 207–228.
- [19] C.J. Wolfe, S.C. Solomon, Shear-wave splitting and implications for mantle flow beneath the MELT region of the East Pacific Rise, *Science* 280 (1998) 1230–1238.
- [20] The MELT seismic team, Imaging the deep seismic structure beneath a mid-ocean ridge: The MELT experiment, *Science* 280 (1998) 1215–1218.
- [21] G. Ekström, A.M. Dziewonski, The unique anisotropy of the Pacific upper mantle, *Nature* 394 (1998) 168–171.
- [22] J.-P. Montagner, B. Romanowicz, Degrees 2, 4, 6 inferred from seismic tomography, *Geophys. Res. Lett.* 20 (1993) 631–634.
- [23] D.P. McKenzie, Finite deformation during fluid flow, *Geophys. J. R. Astron. Soc.* 58 (1979) 689–715.
- [24] N.M. Ribe, Seismic anisotropy and mantle flow, *J. Geophys. Res.* 94 (1989) 4213–4223.
- [25] N.M. Ribe, On the relation between seismic anisotropy and finite strain, *J. Geophys. Res.* 97 (1992) 8737–8747.
- [26] A. Tommasi, Forward modeling of the development of seismic anisotropy in the upper mantle, *Earth Planet. Sci. Lett.* 160 (1998) 1–13.
- [27] A.K. McNamara, P.E. van Keken, S.-I. Karato, Development of anisotropic structure in the Earth's lower mantle by solid-state convection, *Nature* 416 (2002) 310–314.
- [28] J.-P. Montagner, L. Guillot, Seismic anisotropy in the Earth's mantle, in: E. Boschi, G. Ekström, A. Morelli (Eds.), *Problems in Geophysics for the New Millennium*, Ed. Compositori, Rome, 2000, pp. 217–255.
- [29] S.P. Grand, R.D. van der Hilst, S. Widiyantoro, Global seismic tomography: A snapshot of convection in the Earth, *GSA Today* 7 (1997) 1–7.
- [30] A.M. Forte, Seismic-geodynamic constraints on mantle flow: Implications for layered convection, mantle viscosity, and seismic anisotropy in the deep mantle, in: *Earth's Deep Interior: Mineral Physics and Tomography From the Atomic to the Global Scale*, *Geophys. Monogr. Ser. AGU* 117, 2000, pp. 3–36.
- [31] M. McNutt, A.V. Judge, The Superswell and mantle dynamics beneath the South Pacific, *Science* 248 (1990) 969–975.
- [32] A. Cazenave, C. Thoraval, Mantle dynamics constrained by degree 6 surface topography, seismic tomography, and geoid: Inference on the origin of the South Pacific Superswell, *Earth Planet. Sci. Lett.* 122 (1994) 207–219.
- [33] M. McNutt, Superswells, *Rev. Geophys.* 36 (1998) 211–244.
- [34] Y. Ricard, C. Vigny, Mantle dynamics with induced plate tectonics, *J. Geophys. Res.* 94 (1989) 17543–17559.
- [35] B.H. Hager, R.J. O'Connell, A simple global model of plate dynamics and mantle convection, *J. Geophys. Res.* 86 (1981) 4843–4867.
- [36] A.M. Forte, W.R. Peltier, Viscous flow models of global geophysical observables, 1: Forward problems, *J. Geophys. Res.* 96 (1991) 20131–20159.
- [37] A.M. Forte, W.R. Peltier, The kinematics and dynamics of poloidal-toroidal coupling of mantle flow: The importance of surface plates and lateral viscosity variations, *Adv. Geophys.* 36 (1994) 1–119.
- [38] C. DeMets, R.G. Gordon, D.F. Argus, S. Stein, Current plate motions, *Geophys. J. Int.* 101 (1990) 425–478.
- [39] E.R. Engdahl, R.D. van der Hilst, R.P. Buland, Global teleseismic earthquake relocation with improved travel times and procedures for depth determination, *Bull. Seism. Soc. Am.* 88 (1998) 722–743.
- [40] A. Davaille, Hotspots, superswells and mixing in a heterogeneous convecting mantle, *Nature* 402 (1999) 756–760.
- [41] W.H. Press, S.A. Teukolsky, W.T. Vetterling, B.P. Flannery, *Numerical Recipes in Fortran 77*, Cambridge University Press, New York, 1992, pp. 740–744.
- [42] P.K. Smolarkiewicz, L.G. Margolin, MPDATA: A finite-difference solver for geophysical flows, *J. Comput. Phys.* 140 (1998) 459–480.
- [43] A.M. Forte, C. Gaboret, H.K.C. Perry, Seismic-geodynamic constraints on mantle dynamics: Implications for deep continental roots and mantle convective flow below the Pacific Ocean hemisphere, *EOS Trans. AGU* 81 (2000) 48.
- [44] B. Romanowicz, Y. Gung, Superplumes from the core-mantle boundary to the lithosphere: Implications for heat flux, *Science* 296 (2002) 513–516.
- [45] E. Kaminski, N.M. Ribe, A kinematic model for recryst-

- tallisation and texture development in olivine polycrystals, *Earth Planet. Sci. Lett.* 189 (2001) 253–267.
- [46] H. Jung, S.I. Karato, Water-induced fabric transitions in olivine, *Science* 293 (2001) 1460–1463.
- [47] D.R. Toomey, W.S. Wilcock, J.A. Conder, D.W. Forsyth, J. Blundy, E.M. Parmentier, W.C. Hammond, Asymmetric mantle dynamics in the MELT region of the East Pacific Rise: Evidence for asthenospheric return flow, *EOS Trans. AGU* 81 (2000) 48.
- [48] J.A. Conder, D.W. Forsyth, E.M. Parmentier, Asthenospheric flow and the asymmetry of the East Pacific Rise, MELT area, *J. Geophys. Res.* 107 (2002) ETG 1–13.
- [49] J.-P. Montagner, T. Tanimoto, Global upper mantle tomography of seismic velocities and anisotropies, *J. Geophys. Res.* 96 (1991) 20337–20351.
- [50] C.E. Nishimura, D.W. Forsyth, The anisotropic structure of the upper mantle in the Pacific, *Geophys. J. R. Astron. Soc.* 96 (1989) 203–229.
- [51] S.I. Karato, Importance of anelasticity in the interpretation of seismic tomography, *Geophys. Res. Lett.* 20 (1993) 1623–1626.
- [52] S.I. Karato, P. Wu, Rheology of the upper mantle: A synthesis, *Science* 260 (1993) 771–778.
- [53] P.J. Tackley, Mantle convection and plate tectonics: Toward an integrated physical and chemical theory, *Science* 288 (2000) 2002–2007.
- [54] J.G. Marsh et al., The GEM-T2 gravitational model, *J. Geophys. Res.* 95 (1990) 22043–22071.
- [55] A.M. Forte, H.K.C. Perry, Geodynamic evidence for a chemically depleted continental tectosphere, *Science* 290 (2000) 1940–1944.
- [56] A.M. Forte, R.L. Woodward, Global 3D mantle structure and vertical mass and heat transfer across the mantle from joint inversions of seismic and geodynamic data, *J. Geophys. Res.* 102 (1997) 17981–17994.